Phys. Status Solidi B **252,** No. 1, 144–148 (2015) / **DOI** 10.1002/pssb.201400140

physica status solidi b
www.pss-b.com
basic solid state physics

Simulations of electromechanical shape transformations of Au nanoparticles

Vahur Zadin*[,1,2], Arkady V. Krasheninnikov[3], Flyura Djurabekova[2], and Kai Nordlund[2]

[1] Intelligent Materials and Systems Lab, Institute of Technology, Tartu University, Nooruse 1, 50411 Tartu, Estonia
[2] Helsinki Institute of Physics and Department of Physics, P.O. Box 43 (Pietari Kalmink. 2), 00014 University of Helsinki, Finland
[3] Department of Applied Physics, Aalto University, P.O. Box 11100, FI-00076 Aalto, Finland

Received 13 June 2014, revised 29 September 2014, accepted 1 October 2014
Published online 24 November 2014

Keywords finite element simulations, nanoscale contact problem, nanoscale size effects

* Corresponding author: e-mail vahur.zadin@ut.ee, Phone: +372 7374834, Fax: +372 7374825

Metallic nanocrystals can exhibit intriguing properties due to large surfaces specific for low-dimensional objects. Recent experimental observation showed an interesting shape transformation of Au nanoparticle during simultaneous mechanical and electrical load. By applying finite element methods extended to include nanosize effects, we study the mechanisms of such transformations. We utilize fully coupled electro-thermal calculations with the nanoscale correction to the electric and thermal conductivities. The mechanical response of the material is simulated using the elastoplastic material model while the nanoscale mechanical interaction between gold and tungsten particles is simulated using adhesive contact modelling. We observe that Joule heating due to high electric currents increases the temperature of the nanoparticle to the value close to the melting point. In combination with the mechanical stress, this causes significant plastic deformations within the nanoparticle, which can explain the observed shape modification of the latter.

1 Introduction Large surface areas, characteristic to low-dimensional objects can lead to interesting new effects in the nanosystems. Examples are material behaviour dependence from the size [1, 2], increased thermal and electrical resistances in nanosystems [3], effects of the surface stresses, [4] etc.

In a recent experimental study, interesting mechanical behaviour of cobalt and gold nanoparticles being in contact with a tungsten STM tip was observed during simultaneous electrical and mechanical loading [5]. If 10–20 nm nanoparticles were in contact, but without electric current passing through it, no shape modification was noticed. However, if electric current was applied, the shape of Au nanoparticle was significantly elongated forming a sharp tip at the place of the contact. The details of the experiment are to be found elsewhere [5]. Previously, similar experiments were conducted for Al–Cu nanoparticles [6]. In this system, electromigration process was found to be predominant deformation mechanism. In case of Au–W, the material behaviour for Au–W may not necessarily follow the same trend. To understand the deformation mechanisms, the mechanical, electrical and thermal behaviour of the system must be simulated. Recently a suitable simulation approach was implemented and tested [7]. However, the material behaviour was simulated using molecular dynamics, limiting the available time scales to pico- or nanoseconds [7, 8] while the experimental time scales are often significantly longer (seconds) [1, 5]. To overcome this limitation and extend the simulation time scale to comparable level with the experimental studies, we use finite element method (FEM). Application of FEM for nanoscale systems requires modification of available models to include finite size effects. Such modified FEM model was successfully used in Ref. [9] to investigate the surface effects and estimate the effective mechanical properties of nanocomposites. Also, in Ref. [10] it was shown that inelastic deformations and creep can be studied by FEM if the nanostructures are larger than 2 nm in radius.

Material deformation maps for cobalt [11] and different metals [12] suggest plastic deformation or creep to be responsible for material deformation under the expected mechanical loads. The aim of current work is to extend the FEM to include nanoscale size effects and apply it to the Au–W contact problem under coupled electro-thermal and mechanical loading to study the material deformation mechanisms under such conditions.

2 Model of materials and methods

2.1 Simulated system The geometry of the simulated system consists of Au and W plates, forming bulk material, with attached nanoparticles of the same materials as presented in Fig. 1. The shape of the cross-section of nanoparticles was chosen semi-spherical, close to semi-elliptical in the deformed shape due to the surface energy minimization and to be similar to the shape of experimental nanotips. The radius of Au particle is 10 nm (see Fig. 1). Temperature-dependent electric resistivity data for gold are obtained from Ref. [13], for tungsten from Ref. [14] and thermal conductivity is calculated using Wiedemann–Franz law.

The elastic properties of tungsten and gold available in the Comsol Multiphysics Materials Library [15] were used for elastic simulations of the nanoparticles. Very soft mechanical properties of gold cause difficulties in experimental measurements of the plastic parameters of gold, hence, the estimations from available experimental data in the literature were used [16, 17]. The initial yield strength was set to 30 MPa and isotropic tangent modulus to 200 MPa.

2.2 Electric currents and heat transport Current density distribution in the material is calculated using Ohm's law in the differential form:

$$\nabla \cdot [\sigma(T,x)\nabla\phi] = 0, \tag{1}$$

where φ is the potential (V) and $\sigma(T, x)$ conductivity (S m^{-1}), T temperature (K) and x represents spatial coordinates (m). In the bottom of W boundary, we use potential zero boundary condition and in top of the Au boundary, we apply current density so that its integral over the boundary area results in the current I_0.

Temperature distribution in the system is calculated in steady state, as thermal processes in nanoscale systems are very fast compared to the experimental time scale (seconds):

$$\nabla \cdot [\kappa(T,x)\nabla T] = -Q \tag{2}$$

where κ (T, x) is the thermal conductivity (W m^{-1} K^{-1}), $Q = -\mathbf{J} \cdot \bigtriangledown\varphi$ volumetric heat generation rate (W m^{-3}) due to resistive losses and $\mathbf{J}$ current density (A m^{-2}). The material model in Au nanoparticle includes the phase change by using the different conductivities for molten and solid material, available in Comsol Multiphysics [15]. The phases are separated by observing the temperature in the model using smoothed Heaviside function with 300 K smoothing interval (to ensure numerical stability). Finally, if phase change occurs, amount of heat, equal to the latent heat of fusion is removed from the material.

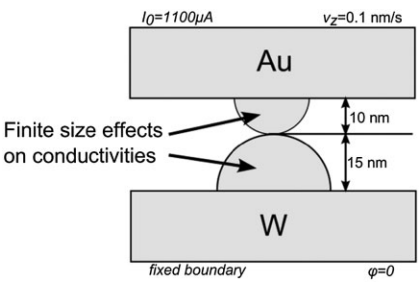

Figure 1 Simulated system and the range of nanoscale size effects.

The finite size effects in the nanoparticles, are characterized using Knudsen number, defined as $Kn = \lambda_e/d$ [18], where λ_e is the mean free path of an electron and d is the diameter of the nanoparticle. If $Kn \ll 1$, the finite size effects are negligible as the physical dimensions of the object are much larger than the mean free path of the electrons. The correction factor $F = F(Kn)$, rising from the finite size effects, is calculated using previously published code [19]:

$$\sigma_{\text{nano}} = F(Kn)\cdot\sigma_{\text{b}} \quad \text{and} \quad \kappa_{\text{nano}} = F(Kn)\cdot\kappa_{\text{b}}, \tag{3}$$

where subscript *nano* corresponds to properties of the nanoparticle and subscript *b* to the properties of bulk. The influence of the finite size effects cannot be underestimated. For example, the conductivity of sub nanometer diameter nanopillars is decreased by more than 10 times.

2.3 Elastoplastic deformation model In these calculations, we assume isotropic materials. The model of a material is expressed as [20]:

$$S = C : \varepsilon_{\text{el}}, \tag{4}$$

where S is the second Piola–Kirchoff stress (Pa), C elastic stiffness tensor and ε_{el} elastic strain. Since the experimental system goes through large deformations, we use finite deformation model. To account plastic deformation, we decompose the deformation gradient tensor F multiplicatively to elastic and plastic parts [20]:

$$F = F_{\text{el}}F_{\text{p}} \tag{5}$$

and remove the plastic deformation from the total deformation gradient $F_{\text{el}} = FF_{\text{p}}^{-1}$. Finally the elastic and plastic Green–Lagrange strain tensors are

$$\varepsilon_{\text{el}} = \frac{1}{2}\left(F_{\text{el}}^{T}F_{\text{el}} - \text{I}\right) \quad \text{and} \quad \varepsilon_{\text{p}} = \frac{1}{2}\left(F_{\text{p}}^{T}F_{\text{p}} - \text{I}\right). \tag{6}$$

We use von Mises yield criterion and the effective stress, von Mises stress, $\varphi(\sigma)$ is defined as [20]:

$$\varphi(\sigma) = \sigma_{\text{mises}} = \sqrt{\frac{3}{2}\,\text{dev}(\sigma) : \text{dev}(\sigma)} = \sqrt{3J_2(\sigma)}, \tag{7}$$

where J_2 is the second deviatoric stress invariant. If von Mises stress reaches yield strength, the material starts to deform plastically. Dislocation interactions during the plastic deformation lead to the material hardening. The

yield strength is a function of the plastic deformation, $\sigma_{ys} = \sigma_{ys}(\varepsilon_{pe})$, where ε_{pe} is effective plastic strain and $\sigma_{ys}(\varepsilon_{pe}) = \sigma_{ys,0} + \sigma_h(\varepsilon_{pe})$ is the plastic deformation-dependent yield strength of the material. The hardening behaviour of the material is captured by increasing the initial yield strength as a function of the local plastic deformation of the material:

$$\sigma_h(\varepsilon_{pe}) = k\varepsilon_{pe} \quad \text{and} \quad \frac{1}{k} = \frac{1}{E_{tiso}} - \frac{1}{E}, \tag{8}$$

where E is the Young's modulus of the material and E_{tiso} is isotropic tangent modulus (slope of the stress–strain curve in plastic deformation part). E_{tiso} describes how the yield strength of the material depends from the plastic deformation and leads in current implementation to constant linear hardening of deformed volume.

2.4 Interface interactions We simulate the Au–W interface by adding thin elastic layer boundary condition between the contact surfaces. It acts as adhesive contact between the particles and uses harmonic oscillator potential to characterize the interaction of the materials. Breaking of the contact is simulated using nonlinear spring coefficient k – it maintains constant value, until certain deformation, u_{max}, is reached. During further deformation, the spring coefficient decreases linearly, until critical deformation u_{break}. Then, k becomes zero and interaction of the materials stops. Contact model is applied using Hooke's law:

$$F = -k \cdot u, \tag{9}$$

where F is the force, k spring coefficient and u displacement between the nanoparticles.

2.5 Simulations In the current study, we do not simulate the compression of Au and W nanoparticles, but assume that this part of the process has already taken place – the simulation started by assuming already deformed Au nanoparticle, pressed to the tungsten surface. Moreover, to simplify the implementation of Eq. (9), the contact area between Au and W was assumed to be flat at tungsten side, not completely spherical. The system was allowed to relax into equilibrium configuration, followed by lifting the Au nanoparticle, by applying constant speed boundary condition ($v_z = 0.1\,\text{nm s}^{-1}$, Fig. 1). At the same time, fully coupled current density and temperature distributions were calculated. Fixed current $I_0 = 1100\,\mu\text{A}$ was used as initial value, with incremental increase (by factors 1, 2 and 3) in following simulations. Currently, the elastoplastic properties of the Au nanoparticle are temperature independent.

Plastic behaviour was modelled only in gold nanoparticle, and the rest of the system was considered elastic (as only the processes in the Au nanoparticle were of interest).

The simulations were conducted using the Comsol Multiphysics package [15]. The material and simulation parameters are summarized in Table 1.

Table 1 Material and simulation parameters.

parameter	value	description
I_0	1100 μA	external current
E_{tiso}	200 MPa	isotropic tangent modulus of Au
$\sigma_{ys,0}$	30 MPa	initial yield strength of Au
κ	$310\,\text{W m}^{-1}\text{K}^{-1}$	thermal conductivity of Au nanoparticle at room temperature
σ	$4.46\times10^7\,(\text{S m}^{-1})$	electric conductivity of Au nanoparticle at 300 K
v_z	$0.1\,\text{nm s}^{-1}$	lifting speed of Au nanoparticle

3 Results and discussion

3.1 Mechanical deformation of the system The von Mises stress distribution in the Au nanoparticle during the simulation is presented in Fig. 2. As predefined deformation and zero initial stress are assumed, the simulation starts with the initial shape relaxation of the Au naoparticle due interaction of Au and W atoms, leading to initial stress distribution (Fig. 2A). The end of this relaxation is considered to be starting point of the simulation ($t = 0$). When the Au nanoparticle is lifted (Fig. 2B and C), it undergoes plastic deformation and gradually reshapes into a previously deformed tip. The contact area between the Au and W decreases during the deformation and neck-like structure forms at the contact due to combined effect of the plastic deformation, nanoparticle shape caused stress concentration and sticking effects between Au and W.

During the stretching, we regain the compressed shape and achieve elongation beyond original height. The elongation of the sample can be explained through dislocation-mediated activities (althoug surface diffusion may also contribute in experimental system). However, as in these simulations mechanical properties of the materials are considered to be temperature independent, we underestimate the shape changes of the tip.

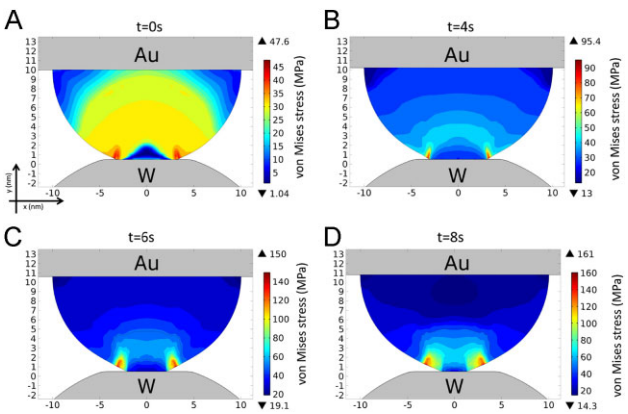

Figure 2 Von Mises stress distribution in the nanoparticles during the simulations. Snapshots A–D demonstrate the progressive deformation of the Au nanoparticle during the lifting.

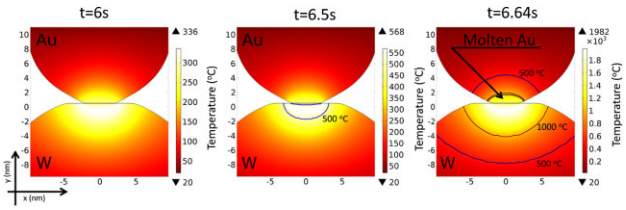

Figure 3 Temperature distributions in the nanoparticles during the simulations. Highest temperature is reached first in the tungsten tip due to its lowest conductive properties.

3.2 Thermal behaviour of the nanoparticles The temperature distribution in the system during the simulation is presented in Fig. 3, where colour represents the temperature and isolines 500, 1000 °C and melting temperature of gold. In figure, three snapshots of the system evolution are presented at $t = 6$, 6.5 and 6.64 s, respectively. In the last snapshot, liquid Au has formed. The increase of the current density needed for sufficient temperature rise is achieved through the decrease of the contact area of the nanoparticles while lifting the Au nanotip. The tungsten tip acts as the main source of the heat as thermal and electric conductivity in W are lower than in Au. However, it is cooled by Au nanoparticle – the maximum temperature is achieved in the tungsten tip, near the interface. As the temperature of the system starts to rise, the electric conductivity becomes lower, leading to higher resistive heating. Finally, if the combined effect of increased current density and higher resistivity of W overcome the cooling effects of the Au nanoparticle at $t \approx 6.64$ s, the melting point of Au is reached and liquid phase forms at the Au–W interface. Further increase of the current density leads to the expansion of the molten area into Au as the heat generation moves towards gold due to the lower conductivity of the liquid phase.

The temperature at the tip of gold nanoparticle during the contact simulation is presented in Fig. 4 for different applied current values. In all cases, at the beginning the temperature rises slowly but increases very fast by the end of the simulation due to combined effect of increase of temperature-dependent resistivity and decrease of contact surface area. While all applied currents were sufficient to cause melting of the Au nanoparticle, significant difference appeared in sensitivity to the contact surface area change.

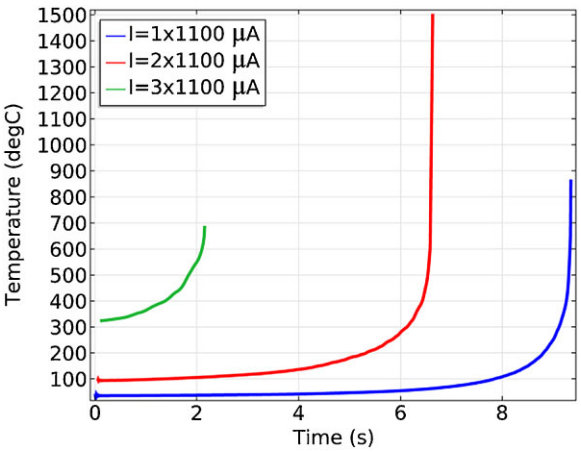

Figure 4 Temperature at the tip of gold nanoparticle during the simulations. Temperature increases due to decreasing contact surface area between the particles.

The lowest applied current (1100 μA, blue line in Fig. 4) caused the fast temperature rise and the sudden melting of the system at the interface between the nanoparticles; the largest current (3×1100 μA, green line in Fig. 4) lead to the fast heating of Au already at the beginning of the simulation leading to early formation of molten phase at ≈2 s. These simulations clearly demonstrated that applied methodology can estimate the melting of the Au nanoparticle for applied currents in the same order of magnitude as in experiment.

4 Conclusions In current study, a system of gold–tungsten nanoparticles is simulated, using the FEM, extended to include nanoscale size effects. The simulations include characterization of the Joule heating caused thermal behaviour of the system. Joule heating due to high electric currents increases the temperature of the nanoparticle close to the melting point. The calculations demonstrated sensitivity to the temperature-dependent electrical and thermal conductivities and stressed the importance of implementation of the finite size effects to the conductivities.

The mechanical interaction between the nanoparticles was simulated using adhesive contact model, with distance-dependent interaction properties. The simulation demonstrated that this kind of interaction leads to the plastic deformation of gold nanoparticle. During the elastoplastic simulations of the system, a clear shape transformation was observed. During the stretching, the Au nanoparticle is deformed beyond the original shape. Combination of high temperature and applied mechanical stress causes significant plastic deformations within the nanoparticle, which can explain the shape modification of the latter. As the plastic deformation model manages to capture the deformation of the system, the elongation of the sample can be understood through dislocation-mediated behaviour, even though surface diffusion and electro-migration may also contribute to the deformation of the particles observed in the experiments.

Acknowledgements Supported by the Tiger University Program of the Information Technology Foundation for Education, Estonian Research Council grant PUT57 and ERDF (European Regional Development Fund). A.V.K. acknowledges support from the Academy of Finland through project No. 263416.

References

[1] G. Dehm, Prog. Mater. Sci. **54**, 664 (2009).
[2] Q. Yu, Z.-W. Shan, J. Li, X. Huang, L. Xiao, J. Sun, and E. Ma, Nature **463**, 335 (2010).
[3] D. Josell, S. H. Brongersma, and Z. Tőkei, Annu. Rev. Mater. Res. **39**, 231 (2009).

[4] H. She and B. Wang, Finite Elem. Anal. Des. **45**, 463 (2009).
[5] L. B. He, B. J. Wang, J. Sun, L. T. Sun, S. X. Mao, and Z. Zhang, to be published.
[6] S. Mei, L. He, X. Wu, J. Sun, B. Wang, X. Xiong, and L. Sun, Nanoscale **6**, 405 (2013).
[7] S. Parviainen, F. Djurabekova, H. Timko, and K. Nordlund, Comput. Mater. Sci. **50**, 2075 (2011).
[8] Z. Qiao, H. Feng, and J. Zhou, Phase Transit. **87**, 59 (2013).
[9] J. Yvonnet, H. L. Quang, and Q.-C. He, Comput. Mech. **42**, 119 (2008).
[10] G. Guisbiers and L. Buchaillot, Nanotechnology **19**, 435701 (2008).
[11] P. M. Sargent, G. Malakondaiah, and M. F. Ashby, Scr. Metall. **17**, 625 (1983).
[12] H. J. Frost and M. F. Ashby, Deformation-mechanism maps: The plasticity and creep of metals and ceramics (Pergamon Press, 1982).
[13] R. A. Matula, J. Phys. Chem. Ref. Data **8**, 1147 (1979).
[14] P. D. Desai, T. K. Chu, H. M. James, and C. Y. Ho, J. Phys. Chem. Ref. Data **13**, 1069 (1984).
[15] http://www.comsol.com/.
[16] L. Condra, J. Svitak, and A. Pense, IEEE Trans. Parts Hybrids Packag. **11**, 290 (1975).
[17] ASM Handbook, Vol. 2: Properties and Selection: Nonferrous Alloys and Special-Purpose Materials, 10th ed. (ASM International, Materials Park, Ohio, 1990).
[18] Z. M. Zhang, Nano/Microscale Heat Transfer (McGraw Hill Professional, New York, 2007).
[19] E. Yarimbiyik, H. A. Schafft, R. A. Allen, M. Zahgoul, and D. L. Blackburn, Implementation of Simulation Program for Modeling the Effective Resistivity of Nanometer Scale Film and Line Interconnects (2006).
[20] A. F. Bower, Applied Mechanics of Solids (CRC Press, Boca Raton, 2009).

